Resilient isolation-structure systems with super-large displacement friction pendulum bearings

Jinping Ou*, Peisong Wu and Xinchun Guan

Key Lab of Structures Dynamic Behaviour and Control of the
Ministry of Education,
Harbin Institute of Technology,
Harbin, 150090, China
Email: oujinping@hit.edu.cn
Email: wupeisong2013@126.com
Email: Guanxch@hit.edu.cn
*Corresponding author

Abstract: This paper presents a super-large displacement friction pendulum bearing (SLDFPB) and isolation system with SLDFPB. SLDFPB has one or several spherical shells of large span and large curvature radius as an integrated sliding isolation layer. Superstructure can sustain large horizontal displacement through relative sliding between large spherical shell and sliding blocks. The proposed SLDFPB has two main advantages: 1) avoid damage of isolation layer during super-strong earthquakes owing to large lateral deformation capability; 2) have better isolation effectiveness because of smaller horizontal stiffness and isolation frequency. This study also investigates mechanical property of SLDFPB including equivalent radius and equivalent friction coefficient. Suggested designed method of SLDFPB is given based on seismic mitigation and reset ability of isolation layer. Two isolation structure systems with multi isolation layers are studied. The results show that large ratio of mass and optimised parameters contribute to good control effect.

Keywords: friction pendulum bearing; sustainable structural system; isolation system; equivalent radius; equivalent friction coefficient.

Reference to this paper should be made as follows: Ou, J., Wu, P. and Guan, X. (2021) 'Resilient isolation-structure systems with super-large displacement friction pendulum bearings', *Int. J. Sustainable Materials and Structural Systems*, Vol. 5, Nos. 1/2, pp.11–34.

Biographical notes: Jinping Ou is an Academician of Chinese Academy of Engineering and Professor of Harbin Institute of Technology. His main research directions are dynamic effects of structural disasters and vibration control, evolutionary behaviour of structural disasters and health monitoring, and performance design of new structural systems for disaster resistance and mitigation.

Peisong Wu is mainly engaged in the research of isolation technology in the field of disaster prevention and mitigation of structures, including the research on the isolation effect of rubber bearing, friction pendulum bearing and other isolation devices with similar principles.

Xinchun Guan is a Professor of Harbin Institute of Technology. He is mainly engaged in the research of intelligent materials and structural systems based on civil engineering, including magnetorheological fluids and their intelligent

vibration damping systems, resin-based magnetostrictive composites and their intelligent vibration damping systems, high performance and intelligent concrete.

This paper is a revised and expanded version of a paper entitled 'Resilient seismic isolated structures with super-large displacement friction pendulum bearings' presented at 2nd International Workshop on Resilience in Nanjing-Shanghai, China, 31 October to 2 November 2018.

1 Introduction

Isolation method belongs to passive control in the classification of structural vibration control. Isolation structure is a resilient structure system to better withstand given ground motion hazard. There are more than one thousand isolation structures built in China in the recent 20 years. These projects proved an effective means of controlling the seismic response of different base isolation devices including rubber bearing and friction pendulum bearing (Standard Institute of Chinese Construction, 2001). Many experimental tests performed that Teflon or PTFE-steel interface is suitable for FPB because the friction coefficient is small and stable under long-term load (Zayas et al., 1989, 1990)

Ghobarah and Ali (1988) applied a set of numerical analysis and experimental tests in order to evaluate isolation stiffness and frequency. They have demonstrated that real isolation frequency of FPB is larger than theoretical frequency from FPB model, and real horizontal stiffness is larger than anticipated value. A new model of FPB subjected to multiple components of excitation was presented by Mosqueda et al. (2004). They performed an investigation on the effects of vertical load. Their new model whose prediction error is smaller than 10% is more applicable than equivalent linear model with viscous damping. Influence of isolation performance from vertical ground motion and separation of sliding block and sliding surface was also studied by Almazán et al. (1998), Landi et al. (2016) and Loghman et al. (2015), respectively.

Some special friction pendulum bearings are also studied. An FPB with variable friction coefficient and the possibility of employing materials with different frictional properties are presented by Panchal and Jangid (2009) and Calvi et al. (2016) respectively. Variable frequency and variable curvature FPB were also indicated by many researchers (Pranesh and Sinha, 2000; Murnal and Sinha, 2002, 2004; Tsai et al., 2003). Double concave FPB is developed to realise variable isolation frequency by Tsai et al. (2005) and Fenz and Constantinou (2006). Seismic performance of triple concave FPB is also verified (Fenz and Constantinou, 2008a, 2008b; Morgan and Mahin, 2010; Tsai et al., 2010; Becker and Mahin, 2012; Dao et al., 2013).

A challenge of vertical or 3D isolation system was also shown during the studies. There is no bearing with large vertical carrying capacity and small vertical stiffness. Vertical isolation bearing which is possible and necessary used in bridges or large-span roofs does not apply to heavy structures.

Another problem of isolation structure is that isolation tall buildings would be collapsed since large displacement of base-isolation layer or large overturning moment of superstructure subjected to super-strong seismic excitation (Du and Li, 2011). Ductility

and resilience of isolation layer will determine seismic performance of isolation structures. Isolation tall building designed under 8.0 intensity earthquakes may collapsed from failure of isolation layer not only have some damage under 8.5 or 9.0 intensity earthquakes (Wu and Ou, 2015). Increasing safety stock and robustness of isolation structure especially isolation layer is significant and relatively easy to realise because of simplex failure mode and certain weakness.

Seismic performance of isolation layer mainly including lateral deform-ability and vertical carrying capability determine the security of isolation structures due to certain failure mode of isolation structures. Horizontal deform-ability of isolation bearings has many restrictions such as small foundation space and limited horizontal stiffness. Size of conventional isolation bearings under bottom columns are usually not larger than cross sectional dimensions of columns. To rubber bearings, lateral radius of rubber layers is directly proportional to thickness of rubber layers due to synchronised growth of lateral shear deformability and capsizing resistance of bearing itself. Horizontal stiffness of rubber bearings calculated from inertia moment scales in proportion to size of isolation bearings. Large rubber bearings are difficult to have good horizontal stiffness and isolation effectiveness.

To solve these restrictions, referring to the theory of friction pendulum bearing, super-large displacement friction pendulum bearings are presented, as Figure 1 shows.

Figure 1 Super-large displacement friction pendulum bearings, (a) without deformation (b) with deformation

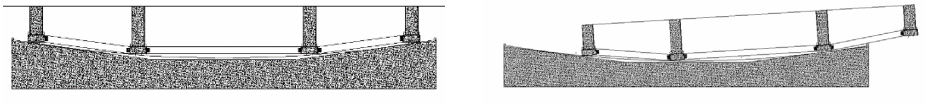

(a) (b)

Different from classic friction pendulum bearing located under each column separately, super-large displacement friction pendulum bearing has one or several spherical shells of large span and large curvature radius above the foundation as an integrated sliding isolation layer. Each super-large displacement friction pendulum bearing acts as an isolation layer. Serving as a huge sliding block, whole superstructure sustains large horizontal displacement through relative sliding between large spherical shell and sliding block under non-deformable frame column.

The spherical shell is integral concreted with high level concrete basement and spherical corrosion resistant plate upwards opening. The sliding block is approximate to flat s stainless steel cylinder with a spherical lower surface. Some low friction materials and antifriction such as Teflon and silicone lubricant are adopted on the surface of spherical shell and sliding block under the columns. These two surfaces have same shape and same radius at corresponding location in order to avoid ductile damage from point contact. Thin edge of the bottom and round rim of sliding block is good for sliding smoothly.

Each sliding block is connected by additional reinforced girders, columns and other jointing elements as the base of superstructure and it's also overlap jointed on the spherical shell by bracket for enhancing punching shear resistance capacity of column

base. Span of spherical shell is larger than sliding superstructure, so that the spherical shell can envelop the superstructure.

Resilience ability of SLDFPB is provided by resultant force of bearing reaction under each column when superstructure is sliding on the spherical shell. As Figure 1 shows, motion of superstructure is rotation and the deformation of isolation layer can be huge. This lateral deformation capability of SLDFPB can satisfy horizontal displacement of isolation layer subjected to severe seismic events.

Horizontal stiffness of SLDFPB and isolation frequency is determined by designed parameters of SLDFPB. Isolation frequency of SLDFPB is much smaller than it of classic FPB due to large radius of SLDFPB. Prominent isolation effect also gives rise to reducing seismic excitation and increasing overturning capability. Each bearing reaction is pressure during earthquakes, and sliding block has no use for resistance to tension. Mass centre of superstructure and stiffness centre of isolation layer are in the same vertical axis, so SLDFPB has good resistance of torsion. Friction force between sliding block and spherical shell fasten superstructure and isolation layer subjected to wind load of design.

2 Seismic performance of super-large displacement friction pendulum bearing

2.1 Mechanical property of super-large displacement friction pendulum bearing

Mechanical property of super-large displacement friction pendulum bearing is different from classic friction pendulum bearing. To isolation devices of sliding type, lateral component of bearing reaction acts as restoring force. In SLDFPB, the direction of bearing reaction for each column is centre of spherical shell. To classic pendulum bearing, each bearing reaction is straight up. Horizontal stiffness of SLDFPB and classic pendulum bearing may have some difference.

Superstructure of conventional pendulum bearing moves along orbit of the bearing and remains horizontal during earthquakes. To isolation structure with SLDFPB, the superstructure rolls around along the orbit and each storey leans towards centre shaft of the orbit. Seismic load not only motivates lateral acceleration due to different directions of motion. Angular acceleration decomposition and rotational kinetic energy make the mechanical property more complex. Stiffness between isolation layer and each storey of superstructure is not zero because of component force of gravity towards each floor from inclination of superstructure.

Equation of motion of a frame structure with n storeys of superstructure and a SLDFPB can be calculated from Lagrange principle when bearing reaction is unknown. Earthquake load is indicated by mass multiply ground acceleration.

Assume that:

1 mass of each storey is distributed evenly

2 superstructure satisfies rigid floor hypothesis

3 columns have infinite vertical stiffness, and superstructure is ‘shear-type’

4 horizontal earthquake in one dimension is considered and vertical acceleration of superstructure is derived from inclination of isolation layer

5 each sliding block has point contact with the sliding surface, and bearing reaction points to centre of spherical

6 ignore damping of superstructure in Lagrange principle.

Figure 2 shows an isolation structure with super-large displacement friction pendulum bearing.

Figure 2 Isolation structure with super-large displacement friction pendulum bearing

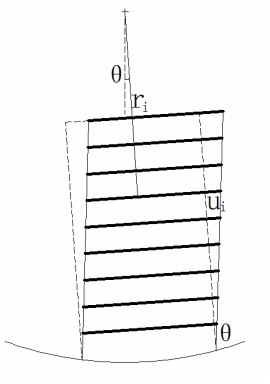

According to Lagrange principle, the equations of motion for the inclination angle of isolation layer θ and horizontal relative displacements u_i between each storey of superstructure and isolation layer are described by

$$\frac{d}{dt}\left(\frac{\partial T}{\partial \dot{\theta}}\right)-\frac{\partial T}{\partial \theta}+\frac{\partial V}{\partial \theta}=\frac{\partial\left(W_f+W_{gm}\right)}{\partial \theta} \tag{1}$$

$$\frac{d}{dt}\left(\frac{\partial T}{\partial \dot{u}_i}\right)-\frac{\partial T}{\partial u_i}+\frac{\partial V}{\partial u_i}=\frac{\partial\left(W_f+W_{gm}\right)}{\partial u_i} \tag{2}$$

In which T is kinetic energy of the system, V is potential energy of the system, W_{gm} is load of ground motion, W_f represents load of friction force.

The results of equations (1) and (2) are shown as equations (3) and (4) when the frame structure is symmetrical.

$$\begin{aligned}&\sum_{i=0}^{n} m_i r_i^2\ddot{\theta}+\sum_{i=0}^{n} I_i\ddot{\theta}+\sum_{i=1}^{n} m_i\left(2u_i\dot{u}_i\dot{\theta}+r_i\ddot{u}_i+u_i^2\ddot{\theta}\right)+\sum_{i=0}^{n} m_i g r_i\sin\theta+\sum_{i=1}^{n} m_i g u_i\cos\theta\\&\quad=m_0\ddot{x}_g(t)r_0\cos\theta+\sum_{i=1}^{n} m_i\ddot{x}_g(t)\left(r_i\cos\theta-u_i\sin\theta\right)+rf\end{aligned} \tag{3}$$

$$m_i\left(\ddot{u}_i+r_i\ddot{\theta}\right)-m_i u_i\dot{\theta}^2+m_i g\sin\theta+k_i u_i-k_i u_{i-1}+k_{i+1}u_i-k_{i+1}u_{i+1}=m_i\ddot{x}_g(t)\cos\theta \tag{4}$$

In which m_i is mass of i^{th} storey which is lumped at the floor level and is allowed to translate exclusively in the same direction as isolation layer; r_i is distance between circle centre of spherical orbit and centre of i^{th} storey; I_i is inertia moment of i^{th} storey; k_i is horizontal stiffness of i^{th} storey; r is radius of spherical orbit; $i = 0$ represents isolation layer. $k_{n+1} = 0$, $u_0 = 0$ which represent unreal stiffness over top storey and relative displacement of isolation layer are convenient for describing the equation.

To solve the complicated nonlinear equations and analyse this system, equations (3) and (4) can be simplified when the angle is small. Assume sin $\theta \approx \theta$, cos $\theta \approx 1$, equations (3) and (4) can be rewritten:

$$\begin{aligned}&\sum_{i=0}^{n} m_i r_i^2 \ddot{\theta} + \sum_{i=0}^{n} I_i \ddot{\theta} + \sum_{i=1}^{n} m_i \left(2u_i \dot{u}_i \dot{\theta} + r_i \ddot{u}_i + u_i^2 \ddot{\theta}\right) + \sum_{i=0}^{n} m_i g r_i \theta + \sum_{i=1}^{n} m_i g u_i \\ &\quad = m_0 \ddot{x}_g(t) r_0 + \sum_{i=1}^{n} m_i \ddot{x}_g(t)(r_i - u_i \theta) + rf\end{aligned} \tag{5}$$

$$m_i \left(\ddot{u}_i + r_i \ddot{\theta}\right) - m_i u_i \dot{\theta}^2 + m_i g\theta + k_i u_i - k_i u_{i-1} + k_{i+1} u_i - k_{i+1} u_{i+1} = m_i \ddot{x}_g(t) \tag{6}$$

Equations (5) and (6) can be linearised because the results of high order items $m_i u_i \dot{u}_i \dot{\theta}$, $m_i u_i^2 \ddot{\theta}$, $m_i u_i \theta \ddot{x}_g(t)$ and $m_i u_i \dot{\theta}^2$ are much smaller than rf, $m_i r_i^2 \ddot{\theta}$, $m_i r_i \ddot{x}_g(t)$ and damping items in the equation. Equations (5) and (6) can be expressed as:

$$\left(\sum_{i=0}^{n} m_i r_i^2 + I_i\right) \ddot{\theta} + \sum_{i=1}^{n} m_i r_i \ddot{u}_i + \sum_{i=0}^{n} m_i g r_i \theta + \sum_{i=1}^{n} m_i g u_i = \sum_{i=0}^{n} m_i r_i \ddot{x}_g(t) + rf \tag{7}$$

$$m_i \left(\ddot{u}_i + r_i \ddot{\theta}\right) + m_i g\theta + k_i u_i - k_i u_{i-1} + k_{i+1} u_i - k_{i+1} u_{i+1} = m_i \ddot{x}_g(t) \tag{8}$$

Equations (9) and (10) describe the equations of motion in which $x_0 = r_0\theta$ represents horizontal displacement of isolation layer. Dividing equation (7) by $\sum_{i=0}^{n} m_i r_i$ makes dimension of each side of the equation to be force.

$$\begin{aligned}&\frac{\sum_{i=0}^{n} m_i r_i^2 + I_i}{\sum_{i=0}^{n} m_i r_i} m_0 \frac{\ddot{x}_0}{r_0} + m_0 \frac{\sum_{i=1}^{n} m_i r_i \ddot{u}_i}{\sum_{i=0}^{n} m_i r_i} + m_0 g \frac{x_0}{r_0} + m_0 \frac{\sum_{i=1}^{n} m_i g u_i}{\sum_{i=0}^{n} m_i r_i} - \frac{m_0 r}{\sum_{i=0}^{n} m_i r_i} f \\ &\quad = m_0 \ddot{x}_g(t)\end{aligned} \tag{9}$$

$$m_i \left(\ddot{u}_i + r_i \frac{\ddot{x}_0}{r_0}\right) + m_i g \frac{x_0}{r_0} + k_i u_i - k_i u_{i-1} + k_{i+1} u_i - k_{i+1} u_{i+1} = m_i \ddot{x}_g(t) \tag{10}$$

In equation (9), analogous to classic friction pendulum bearing, ratio between $\ddot{x}_0$ and x_0 is different. The equivalent radius of SLDFPB r_e is defined by this ratio and it represents the relation between isolation frequency and radius of isolation bearing. When mass and span of each storey is considered as same value, equivalent radius depends solely on radius of isolation layer, number of storey and span of storey.

$$r_e = \frac{\sum_{i=0}^{n} m_i r_i^2 + I_i}{\sum_{i=0}^{n} m_i r_i} = r_0 - \frac{1}{2}nh + \frac{L^2 + (nh)^2 + 2nh^2}{12\left(r_0 - \frac{1}{2}nh\right)} \tag{11}$$

In which $I_i = \frac{1}{12} m_i L^2$, L is span of the frame. For a certain structure, the smallest equivalent radius appears when the height of superstructure is somewhat larger than the radius of spherical orbit.

Figure 3 shows equivalent radius of a frame structure with 6 storeys whose storey height h = 3 m, framing span L = 26.3 m, depth of isolation layer h_0 is from 0.5 to 5 m. Based on the theory of friction pendulum bearing, $r_p = \frac{g}{\omega_1^2}$ represents the equivalent radius calculated from nature period of the isolation system.

Figure 3 Equivalent radius of a frame structure with six storeys

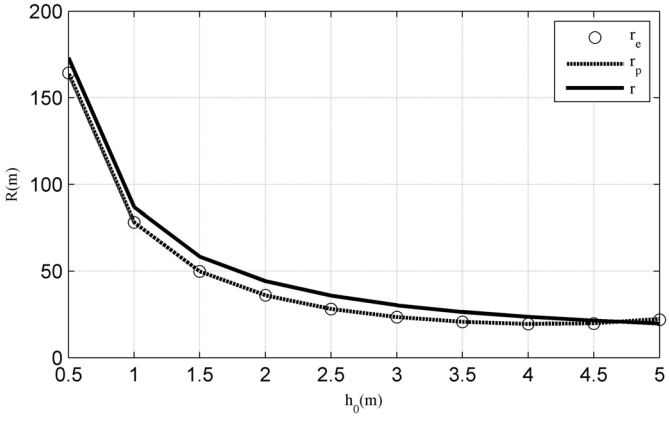

Figure 3 shows that the result of equivalent radius r_e is consistent with the equivalent radius r_p. r_e is unequal to the radius of spherical orbit. Nature period of isolation system can be evaluated accurately by equivalent radius r_e. The equivalent radius from equation (11) can be used in design.

Figure 4 is the equivalent radius of different isolation layer used in a group of frame structures with different storeys whose storey height h = 3 m, framing span L = 26.3 m. SLDFPB has different isolation frequency when the altitude distribution of storey mass is different. Both radius of spherical orbit and equivalent radius decrease with depth of isolation layer h_0 in same situation in accordance to geometrical relationship of spherical shell orbit and equation (11), respectively. To a SLDFPB with certain span, equivalent radius r_e is expressed as a function of height of superstructure. r_e is smaller than r when height of superstructure is smaller than radius of spherical orbit. Equivalent radius is possible to exceed radius of spherical shell when the height of structure is somewhat larger than the radius. This is a relevant aspect to be taken into account in design.

Figure 4 Equivalent radius of different frame structures

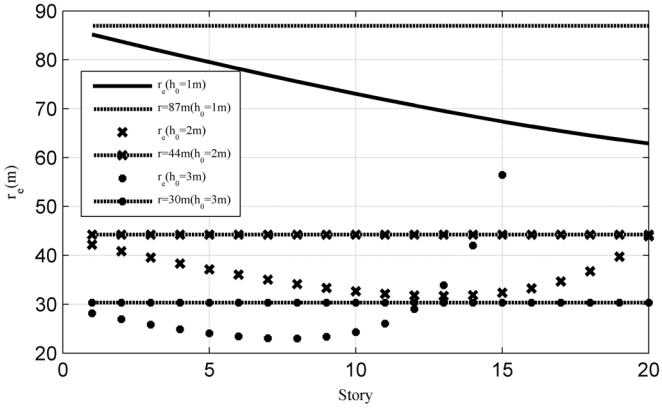

Based on Coulomb friction principle, friction coefficient in static and dynamic conditions is constant. $f=-\mathrm{sgn}(\dot{x}_0)\sum\mu N$, items about friction force in equation of motion is determined by signum function of velocity of isolation layer and algebraic sum of bearing reaction when friction coefficient and curvature radius is constant on the surface of the spherical shell. However, result of bearing reaction is hard to obtain from Lagrange principle.

To single-span multi-storey frame structure which is a statically determinate structure, following D'Alembert's principle, lateral and vertical resultant force is equal to zero when friction force is zero. The final expression of equation of equilibrium is

$$\begin{bmatrix}\cos(\theta-\alpha') & \cos(\theta+\alpha')\\ \sin(\theta-\alpha') & \sin(\theta+\alpha')\end{bmatrix}\begin{bmatrix}N_1\\N_2\end{bmatrix}=\begin{bmatrix}\sum m_i g+\sum m_i r_i\sin(\theta+\alpha_i)\ddot{\theta}\\ \sum m_i\ddot{x}_g-\sum m_i r_i\cos(\theta+\alpha_i)\ddot{\theta}\end{bmatrix} \tag{12}$$

Each bearing reaction can be simplified as

$$\begin{bmatrix}N_1\\N_2\end{bmatrix}=\left(\frac{m}{\sin 2\alpha'}\right)\begin{bmatrix}\sin(\theta+\alpha')'\,\mathrm{g}-\cos(\theta+\alpha')'\,\ddot{x}_g+\sum\dfrac{r_i\cos(\alpha_i-\alpha')}{n}\ddot{\theta}\\ -\sin(\theta-\alpha')\mathrm{g}+\cos(\theta-\alpha')\ddot{x}_g-\sum\dfrac{r_i\cos(\alpha_i+\alpha')}{n}\ddot{\theta}\end{bmatrix} \tag{13}$$

In which α' represents angle between vertical direction and direction from sliding block to centre of spherical orbit; N_1, N_2 represent bearing reactions of columns; α_i represents angle between vertical direction and direction from edge of i^{th} storey to centre of spherical shell. Algebraic sum of bearing reaction is expressed in terms of the result of static condition.

$$N_1+N_2\approx\sum_{i=0}^{n}m_i g\frac{r_0}{r} \tag{14}$$

Algebraic sum of bearing reaction for status of moving changes a little when friction force is small, so that small redistribution of each bearing reaction can be neglected. This conclusion also applies to statically indeterminate structures such as multi-span frame

structures because uneven distribution of each bearing reaction has less influence on algebraic sum of bearing reaction. The equation of motion can be described by replacing bearing reaction of original position. Plug the result into equation (9), equation of motion for isolation layer is given by

$$\frac{\sum_{i=0}^{n} m_i r_i^2 + I_i}{\sum_{i=0}^{n} m_i r_i} m_0 \frac{\ddot{x}_0}{r_0} + m_0 \frac{\sum_{i=1}^{n} m_i r_i \ddot{u}_i}{\sum_{i=0}^{n} m_i r_i} + m_0 g \frac{x_0}{r_0} + m_0 \frac{\sum_{i=1}^{n} m_i g u_i}{\sum_{i=0}^{n} m_i r_i} + \frac{\sum_{i=0}^{n} m_i r_0}{\sum_{i=0}^{n} m_i r_i} \mu m_0 g \operatorname{sgn}(\dot{x}_0) = m_0 \ddot{x}_g(t) \tag{15}$$

When superstructure is regarded as rigid body, equation (15) can be rewritten as similar form of equation of motion for friction pendulum bearing.

$$\frac{r_e}{r} m_0 \ddot{x}_0 + \mu_e m_0 g \operatorname{sgn}(\dot{x}_0) + \frac{m_0 g}{r} x_0 = m_0 \ddot{x}_g \tag{16}$$

In which,

$$r_e = \frac{\sum_{i=0}^{n} m_i r_i^2 + I_i}{\sum_{i=0}^{n} m_i r_i} < r \tag{17}$$

$$\mu_e = \frac{\sum_{i=0}^{n} m_i r_0}{\sum_{i=0}^{n} m_i r_i} \mu > \mu \tag{18}$$

r_e and μ_e is defined by the same relation from frequency and damping ratio to radius and friction coefficient of isolation bearing. Equivalent radius r_e is usually smaller than radius of spherical shell and equivalent friction coefficient μ_e is larger than friction coefficient of spherical shell. The equation of motion shows that SLDFPB and conventional FPB have same ratio between restoring force and seismic excitation. SLDFPB has larger ratio between friction force and seismic excitation, but fewer ratio between inertia force and earthquake load.

Equation (19) describes the force transfer coefficient of single degree of freedom subjected to force vibration (Chopra, 2001).

$$TR = \frac{1}{\sqrt{\left(1-\beta^2\right)^2 + (2\zeta\beta)^2}} \sqrt{1+(2\zeta\beta)^2} \tag{19}$$

In which β is frequency ratio of transfer force to the load, ζ is damping ratio.

To isolation structure, small isolation frequency and large isolation damping lead to weak seismic mitigation. Large r_e and small μ_e are beneficial to reduce seismic load of superstructure.

Because number, size and distance of column are unrelated to the equation of motion, SLDFPB can maintain its mechanical property even if several columns separate from spherical shell caused by enormous deformation of isolation layer or bad contact of sliding block. Local failure only leads to redistribution of bearing reaction. SLDFPB has a stable performance of mechanical property.

2.2 Seismic performance of isolated structure with super-large displacement friction pendulum bearing

Seismic performance of isolation structure with different parameters of SLDFPB subjected to rare and super-rare earthquakes are studied. A frame structure of 30 storeys with dimensions of 27 m by 27 m in plan and 90 m in height is idealised in Figure 5. Natural period and damping ratio of this structure is 1.75 s and 0.05 respectively.

Figure 5 Frame structure of 30 storeys

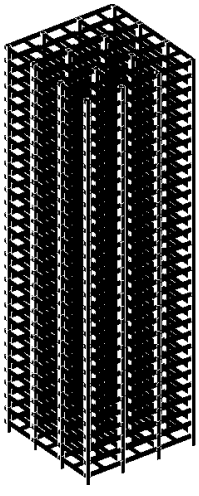

Main parameters of SLDFPB are depth and friction coefficient. Depth of SLDFPB for example 0.5 m to 1 m, determines radius of spherical shell and natural frequency of the bearing. In order to save space of basement, depth of SLDPFB should not exceed the height of each storey. Friction coefficient is determined by materials of interface. Generally, friction coefficient of liquid or graphite lubricant can reach 0.01; friction coefficient of steel and concrete is near 0.02; friction coefficient of conventional friction pendulum bearing is usually between 0.02 and 0.1.

Model of multiple degrees of freedom are built in MATLAB to simulate time history analysis of isolation structure. Superstructure of isolation structure is simplified to elastic 'shear-type' model based on equation (10). It has to be noted that the stiffness between isolation layer and each storey of superstructure is not zero. Damping matrix is calculated in accordance to Rayleigh damping model. Mass matrix and stiffness matrix of isolation

structure as well as first and second mode frequency of superstructure are used in order to simulate valid damping matrix of superstructure. It is believed that the results of time history analysis remain acceptable because damping force of isolation layer has much less influence than friction force. Friction force of the sliding surface follows Coulomb's friction principle. SLDFPB is idealised through lumped mass connected by translational springs to simulate horizontal stiffness of isolation layer based on equation (15). The classical Runge-Kutta method was adopted for the nonlinear numerical testing of SLDFPB so that stick-slip motion of isolation layer can be considered.

Five natural ground motions which are summarised in Table 1 and two artificial seismic waves are used in time history analysis to review the earthquake-resistant performance. Each ground motion has been calculated in different peak ground accelerations which represent different intensities of earthquakes.

Table 1 Five real ground motions used in time history analysis

	Earthquake event	*Mw*	*Station*	*Component*
Ground motion 1	Chi-Chi – Taiwan, 1999	7.62	HWA043	CHICHI/HWA043-FN
Ground motion 2	Chi-Chi – Taiwan, 1999	7.62	TCU038	CHICHI/TCU038-FP
Ground motion 3	Kocaeli – Turkey, 1999	7.51	Atakoy	KOCAELI/ATK-FP
Ground motion 4	Loma Prieta, 1989	6.93	Salinas-John & Work	LOMAP/SJW-FP
Ground motion 5	Loma Prieta, 1989	6.93	Agnews State Hospital	LOMAP/AGW-FP

Depth of SLDFPB used in time history analysis is 0.5 m, 0.6 m, 0.7 m, 0.8 m, 0.9 m and 1.0 m. According to geometrical relationship between radius and span, radius of spherical shell orbit is 225 m, 187 m, 161 m, 141 m, 125 m and 113 m respectively. On the basis of Equation 18, equivalent radius of spherical shell is 84 m, 148 m, 122 m, 104 m, 90 m and 79 m respectively. Mean value of the response subjected to seven ground motions is shown as follows.

Inter storey draft ratio of isolation structure with SLDFPB of different depths is outlined in Figure 6. Friction coefficient in this group of models is 0.01. Small inter-storey draft ratio represents outstanding seismic mitigation. The response of inter-storey draft ratio shows that SLDFPB have great isolation effect because of their large vertical carrying capacity and small horizontal stiffness. This frame structure has some plastic damage subjected to seismic excitation whose PGA is 0.2 g. With SLDFPB, it can survive subjected to earthquake whose PGA is 0.62 g. Benefited from large space in isolation layer, SLDFPB could have a large radius of bearing and a larger equivalent radius. Its horizontal stiffness could be small enough and structures can withstand subjected to severe seismic events. Because of elastic time history analysis of superstructure, inter-storey draft ratio of each model has almost linear increase with large PGA. The reason of relatively large inter-storey draft ratio and inapparent means of controlling the response subjected to ground motions with small intensity is movement impeding of isolation layer from friction force.

Depth of isolation layer h_0 has a prominent influence on seismic mitigation. SLDFPB with smaller depth of isolation layer h_0 has a larger equivalent radius r_e, a larger isolation period and better isolation effect. When depth of isolation layer is 0.5 m, the superstructure maintains low plastic range even subjected to ground motion whose PGA arrives 0.62 g. Isolation effect reduces sharply with increase of h_0. This is one of major determinant of design depth h_0.

Figure 6 Inter-storey draft ratio of isolation structure with SLDFPB of different depths

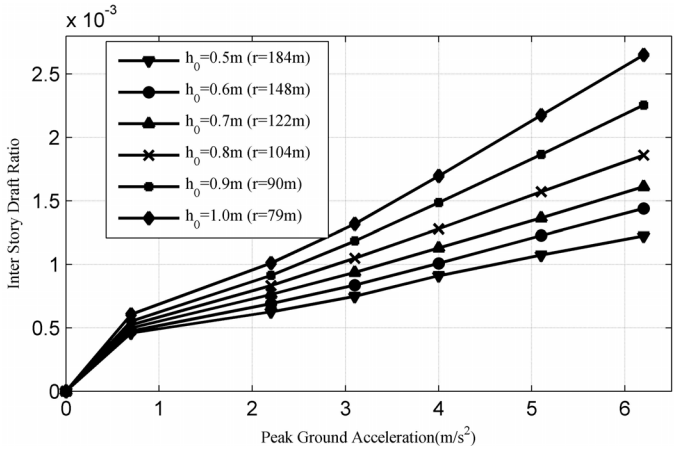

Figure 7 depicts inter-storey draft ratio of isolation structure with SLDFPB of different friction coefficient. Depth of isolation layer in this group of models is 0.5 m. It has an excellent isolation effectiveness when the friction coefficient is small subjected to very rare earthquakes. Different friction coefficients of spherical shell give rise to wide difference of inter-storey draft ratio. The structure may not survive severe seismic events when friction coefficient is a little large.

Figure 7 Inter-storey draft ratio of isolation structure with SLDFPB of different friction coefficient

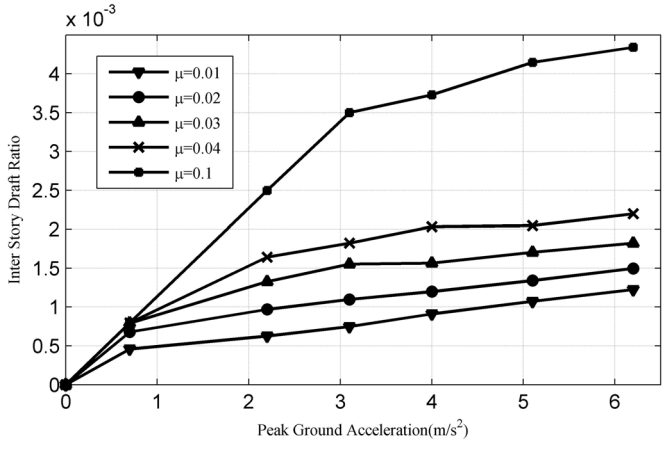

Increasing tendency between PGA and inter storey draft ratio is approximately bilinearity. Under frequent earthquakes whose PGA is 0.07 g, maximum static friction force is always larger than seismic load so that still isolation layer leads to similar inter storey draft ratio and indistinctive isolation effect. The isolation layer has more chance of movement and normal operation condition during stronger seismic excitation so that isolation effect is close to expected value and inter-storey draft ratio grows slowly. Uniformity variation of isolation effect in normal operation condition with friction coefficient corresponds to the relation between force transfer coefficient and damping.

Large friction coefficient such as 0.1 brings about the phenomenon that the sliding block begins to slip only when the resultant force of isolation layer including inertia force is larger than breakaway force which is equal to the weight of superstructure multiplied by the equivalent friction coefficient. This situation could not occur during frequent earthquakes, and it is hard to realise during moderate earthquakes because ground acceleration is difficult to maintain high level in most time. SLDFPB with large friction coefficient can be controllable only subjected to severe seismic excitation. As a result, curve of large friction coefficient has obviously nonlinearity.

In view of seismic behaviour of SLDFPB during moderate earthquakes, sliding surface with small friction coefficient such as Teflon and graphite lubricant is recommended. Taking seismic mitigation subjected to very rare earthquakes into consideration, SLDFPB with relatively small friction coefficient is appropriate.

Maximum displacement of isolation layer with SLDFPB of different depths is depicted in Figure 8. Friction coefficient in this group of models is 0.01. This result in Figure 8 which is maximum value subjected to seven ground motions represents worst-case value of lateral deformation of isolation layer. Safety of isolation layer is under the condition of horizontal displacement. Maximum displacement of SLDFPB subjected to super-strong earthquakes is larger than 1.2 m but much smaller than the deformation capability of SLDFPB. The structure will not destroy due to large deformation of SLDFPB.

Depth of SLDFPB has insensitive influence on the horizontal displacement. In general, small depth of SLDFPB leads to small stiffness of isolation layer and large horizontal displacement. The randomness of this response cause that there is little direct reaction between the response and isolation effect. There is a phenomenon during seismic excitation that superstructure may stick at random location when the seismic load is not strong. The slipping direction of superstructure is also random so that the deformaiton of SLDFPB may continue to increase and isolation capability is also maintained during a finite time. The response difference of small intensity of the ground motions is quite small due to mainly stick situation. The response randomness of large PGA is inapparent because stick situation is uncommon. The response is also nonlinear increase with PGA owing to the same reason.

Figure 8 Maximum displacement of isolation layer with SLDFPB of different depths

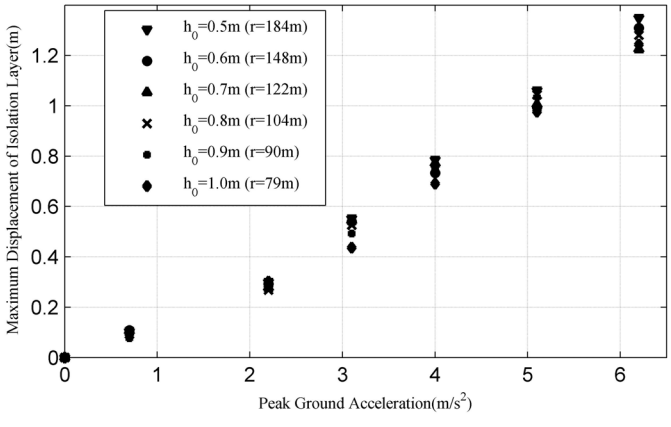

Figure 9 exhibits maximum displacement of isolation layer with SLDFPB of different friction coefficient when depth of isolation layer is 0.5 m. This result is also maximum value subjected to seven ground motions. Friction coefficient has strong influence on horizontal displacement. Overall, the deformation of isolation layer reduces with the increase of friction coefficient. The response randomness of large friction coefficient is obvious due to stick situation of SLDFPB. Small friction coefficient is beneficial to maintaining normal operation condition.

Figure 9 Maximum displacement of isolation layer with SLDFPB of different friction coefficient

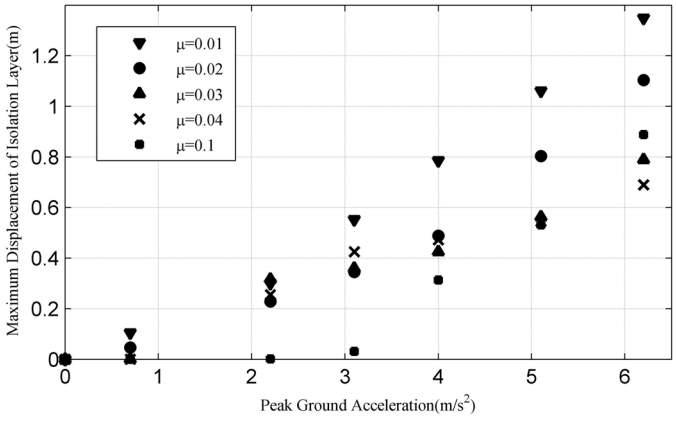

Reset ability is one of the key points in SLDFPB design. Residual displacement of the two groups of models is shown in Figures 10 and 11. Residual displacement is a random variable determined by the status of the bearing during the end of ground motion subjected to different ground motion. It has similar trend as maximum displacement of SLDFPB and maximum theoretical residual displacement. Both of them are determined by friction coefficient and equivalent radius. Maximum theoretical residual displacement is defined as the position where restoring force is equal to friction force. SLDFPB with large depth of isolation layer h_0 and small equivalent radius r_e has a small maximum displacement and small maximum theoretical residual displacement, so the residual displacement is more probably small. Small depth of isolation layer is the design strategy of SLDFPB.

To a SLDFPB with small friction coefficient, large maximum displacement will not restrict residual displacement; both maximum theoretical residual displacement and residual displacement reduce with decrease of friction coefficient. On the contrary, to a SLDFPB with large friction coefficient, residual displacement is determined by small maximum displacement; both maximum displacement and residual displacement increase with decrease of friction coefficient. With the increasing of friction coefficient, residual displacement raises first and then fall. Only considering reset ability separately, small friction coefficient such as 0.01 is recommended. If processing technology of friction coefficient is not within the design bearing capacity, a large friction coefficient for example 0.1 is receivable.

Figure 10 Residual displacement of isolation layer with SLDFPB of different depths

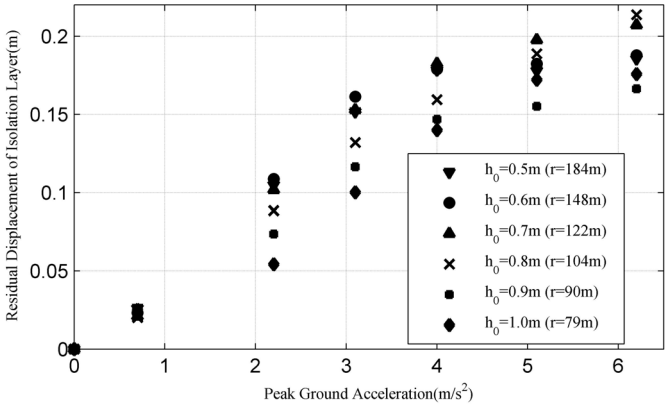

Figure 11 Residual displacement of isolation layer with SLDFPB of different friction coefficient

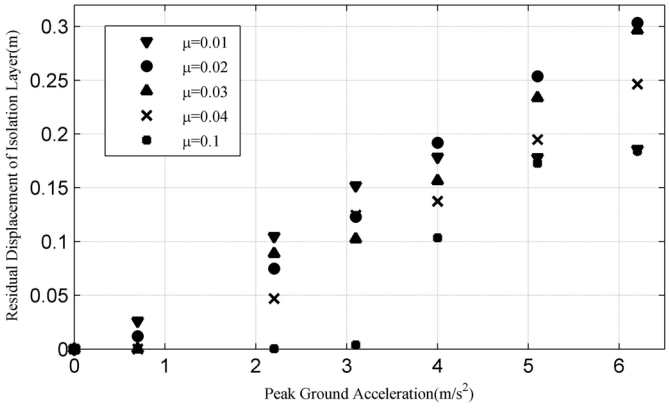

Figure 12 Maximum acceleration of first storey with SLDFPB of different depths

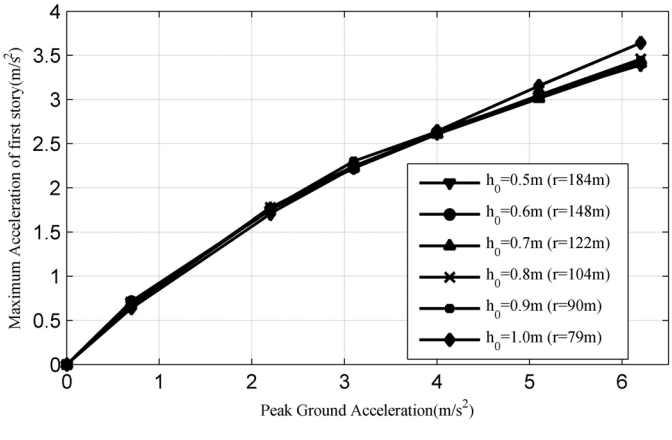

Maximum horizontal acceleration of first storey with SLDFPB of different depths is illustrated in Figure 12. This response can reflect seismic mitigation to some extent. First floor acceleration is always less than ground acceleration. Good isolation effect makes a large difference between first floor acceleration and ground acceleration subjected to severe seismic excitation.

Considering the protection of non-structural elements, maximum acceleration of first storey with SLDFPB of different friction coefficient is shown in Figure 13. Depth of isolation layer in this group of models is 0.5 m. There is apparent difference between each curve. Small friction coefficient is corresponding to small first floor acceleration and weak isolation effectiveness. There is similar conclusion from first floor acceleration and inter-storey draft ratio.

Figure 13 Maximum acceleration of first storey with SLDFPB of different friction coefficient

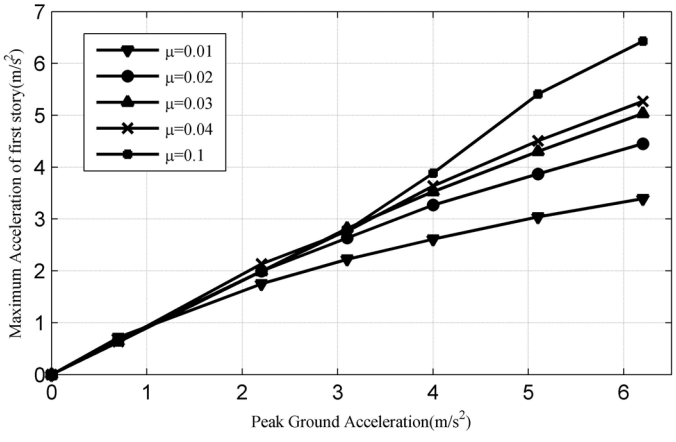

Figure 14 Tangential of inclination of isolation layer with SLDFPB of different depths

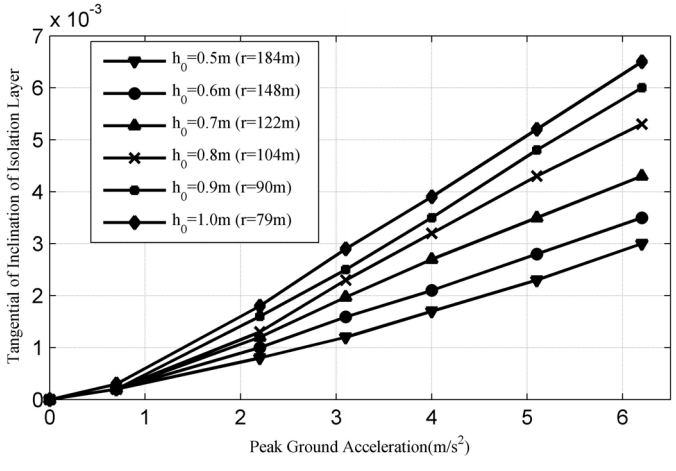

Figure 14 plots tangential of inclination of isolation layer with SLDFPB of different depths. Inclination angle of superstructure θ is tiny even during super-strong earthquakes, so that there's little influence of rotation motion for personnel and equipment. Horizontal

displacement of SLDFPB and radius of spherical shell determine the skew angle of superstructure. Therefore, large PGA and large depth enhance the slope.

Figure 15 shows tangential of inclination of isolation layer with SLDFPB of different friction coefficient. To SLDFPBs with same depth, mean of maximum inclination of isolation layer is determined by mean of maximum horizontal displacement. Randomness of mean is smaller than it of maximum value so that regularity in Figure 15 is more apparent than Figure 9.

Figure 15 Tangential of inclination of isolation layer with SLDFPB of different friction coefficient

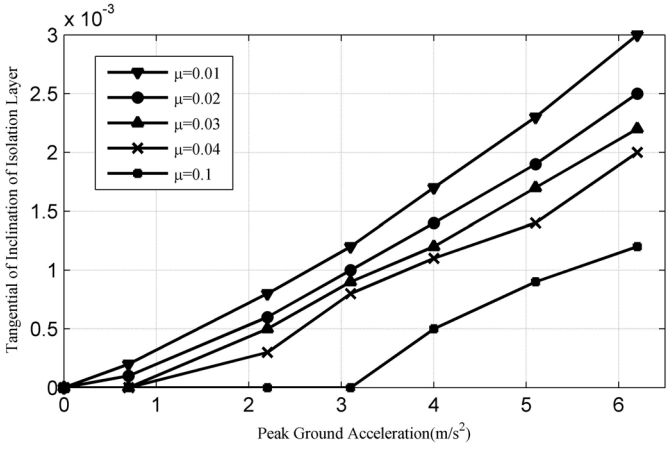

Maximum vertical displacement of superstructure which represents vertical influence of rolling motion form is shown in Figures 16 and 17. Maximum vertical displacement of superstructure appears at the edge of the frame. This response is mainly caused by the inclination of isolation layer and relative displacement between isolation layer and each floor. The relative horizontal displacement is much smaller than the span so that tendency of vertical displacement of superstructure consists with the trend of inclination of isolation layer.

Figure 16 Maximum vertical displacement of superstructure with SLDFPB of different depths

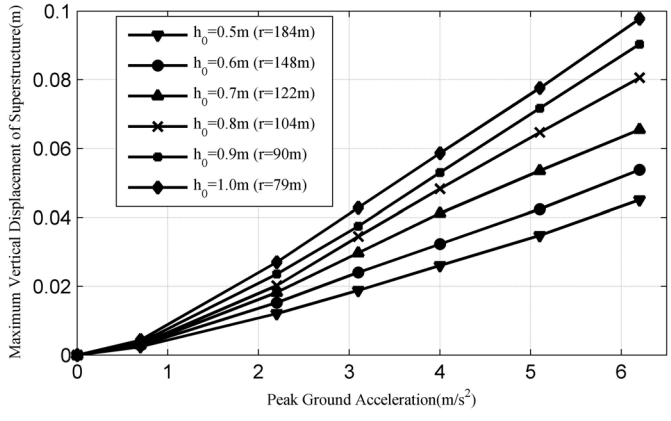

Figure 17 Maximum vertical displacement of superstructure with SLDFPB of different friction coefficient

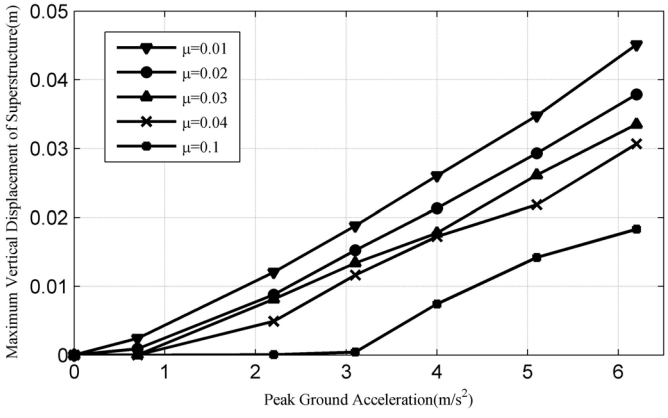

Figure 18 Maximum vertical acceleration of superstructure with SLDFPB of different depths

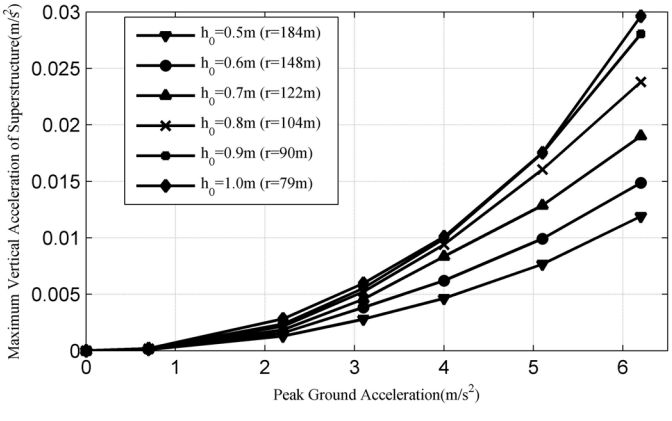

Figure 19 Maximum vertical acceleration of superstructure with SLDFPB of different friction coefficient

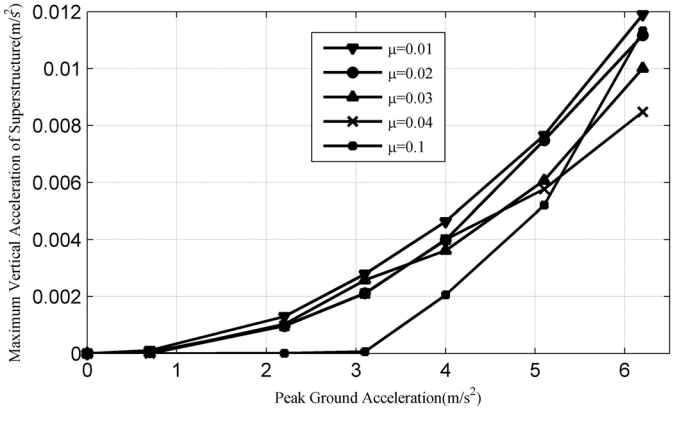

There are maximum vertical acceleration of superstructure with SLDFPB of different depths and different friction coefficient in Figures 18 and 19. Maximum vertical acceleration of superstructure is also inconspicuous. There is no strong sense of weightless or overweight subjected to super-strong earthquakes.

Considering seismic resistance of structures of isolation structure, small friction coefficient will lead to small maximum residual displacement of isolation bearing and good isolation effect, large equivalent radius is good for keeping away from frequency of ground motion. Structures with SLDFPB which has optimal design parameters can maintain quasi-elastic subjected to super-strong earthquakes.

3 Seismic performance of prefabricated structure systems with multiple isolation layers

Referring to the theory of tuned mass damper, super-large displacement friction pendulum bearing applies to combine isolation with energy-dissipation technique. A new system which has two isolation layers in the top and base respectively is studied, as Figure 20(a) shows. The main advantage of base isolation layer is to make sure a quasi-elastic system subjected to rare earthquakes. Top isolation layer working as tuned mass damper can dissipate the earthquake. Displacement of the TMD is not huge because of the large mass.

Figure 20(b) shows isolation structure with multi isolation layers. High rise structure divides into several modules which has some storeys. Each module is a whole isolation structure with SLDFPB. Each module can remain resilience during rare earthquakes so that this structure system has good resilience ability. The complicated structure with many degrees of freedom and modes of vibration simplifies to several degrees of freedom and evident modes of vibration.

Figure 20 Schematic diagram of prefabricated-building system with multiple isolation layers, (a) isolation structure with two isolation layers (b) isolation structure with multi isolation layers

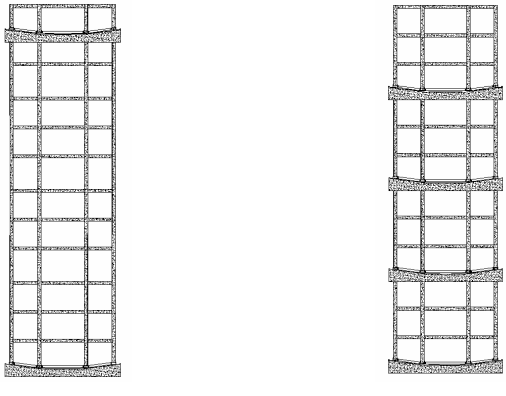

(a) (b)

Optimised parameters of isolation system with two isolation layers are designed by

$$f_\omega = \frac{1}{1+\mu_m} \tag{20}$$

$$\zeta_c = \sqrt{\frac{3\mu_m}{8(1+\mu_m)}} \tag{21}$$

In which f_ω is frequency ratio of top isolation layer, μ_m is mass ratio of top isolation layer, ζ_c is damping ratio of top isolation layer.

According to same energy dissipation in one hysteretic loop, the relation between equivalent friction coefficient and damping ratio is described by

$$\zeta_c = \frac{E_D}{2\pi k d_{\max}^2} = \frac{\mu_e r_e}{2\pi d_{\max}} \tag{22}$$

Optimised size of toping isolation layer and friction coefficient of top spherical orbit can be determined from equation (16), (20), (21) and (22).

Super-large displacement friction pendulum bearings also apply to isolation structure with multi isolation layers. Seismic response of an example of this system and two examples of isolation structure with two isolation layers are compared and shown in Table 3. Figure 21 is the superstructure with 20 storeys whose natural period is 2.1 s. Table 2 lists parameters of SLDFPB in the examples.

Figure 21 Superstructure with 20 storeys in the examples

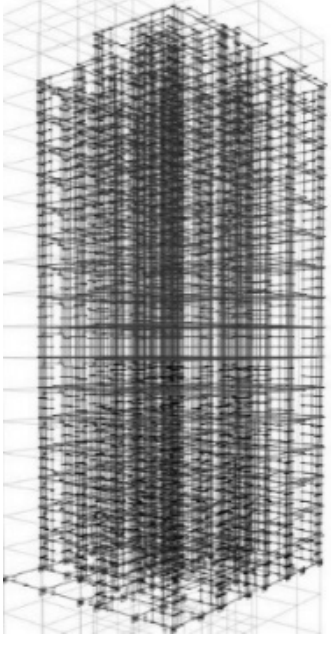

Table 2 Parameters of SLDFPB in the examples

	System A with two isolation layers	*System B with two isolation layers*	*System C with multi isolation layers*
Location (num. of storey)	20	18	1, 7, 14
Depth (m)	1.237	0.756	1
Friction coefficient	0.0116	0.0127	0.01

Table 3 Seismic response of three isolation systems

System	*System A with two isolation layers*		*System B with two isolation layers*		*System C with multi isolation layers*		*System D with one isolation layer*	
PGA	*0.4 g*	*0.6 g*	*0.4 g*	*0.6 g*	*0.4 g*	*0.6 g*	*0.4 g*	*0.6 g*
Max disp. of base isolation layer (m)	0.507	0.953	0.507	0.937	0.530	1.029	0.613	1.124
Residual disp. of base isolation layer (m)	0.116	0.144	0.122	0.157	0.093	0.163	0.091	0.213
Max disp. of top isolation layer (m)	0.359	0.569	0.263	0.458	0.008	0.014	-	-
Residual disp. of top isolation layer (m)	0.038	0.087	0.057	0.078	0.001	0.003	-	-
Inter-storey draft ratio	1/303	1/214	1/545	1/344	1/294	1/203	1/325	1/212
Max disp. of mid isolation layer (m)	-	-	-	-	0.010	0.012	-	-
Residual disp. of mid isolation layer (m)	-	-	-	-	0.002	0.002	-	-

Figure 22 Inter-storey draft ratio of four systems

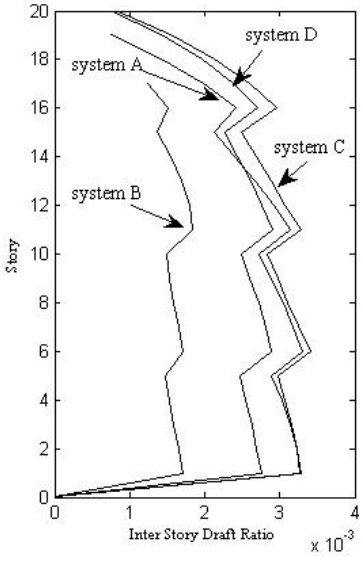

Seismic resistance of isolation structures with two or multi isolation layers are indicated from Table 3. Maximum displacement of base isolation layer in system A and B is similar, so they have similar isolation effects. Only system B has better control effect than based isolation structures with SLDFPB. Large ratio of mass and optimised parameters contributes to good control effect. Design of isolation layers has a large influence on the seismic resistance of structures. One group of inter-storey draft ratio is shown in Figure 22. Inter-storey draft ratio of each storey in system B is smaller and closer, and seismic performance of each storey is fully exerted.

4 Super-large displacement translation friction pendulum bearing

Another kind of super-large displacement friction pendulum bearing is studied, as Figure 23 shows. There are a group of spherical shells with large radius and span in the isolation layer. Several sliding frames used as basement or mechanical floor act as sliding block of the friction pendulum bearing. This bearing and FPB have similar mechanical property because there's no rotation. Subjected to earthquakes, superstructure will move along its arc and keep upright. All these super-large displacement friction pendulum bearings are studied by Key Lab of Structures Dynamic Behaviour and Control of the Ministry of Education, Harbin Institute of Technology.

Figure 23 Super-large displacement translation friction pendulum bearing, (a) without deformation (b) With deformation

(a) (b)

5 Conclusions

Two kinds of super-large displacement friction pendulum bearings and two isolation systems with multi isolation layers are introduced. The study has focused on introducing the concept of super-large displacement friction pendulum bearing and the resilient-isolated structural system of SLDFPB, establishing the mechanical model of SLDFPB with the new isolation systems, analysing nonlinear time history response and optimising parameters of aseismic design.

The conclusions are as follows:

1 Mechanical property of super-large displacement friction pendulum bearing is different from classic friction pendulum bearing. Equivalent radius of SLDFPB is smaller than radius of spherical shell, and equivalent friction coefficient is larger than friction coefficient of contact surface. The restoring force, earthquake load and isolation frequency of SLDFPB is same as the results of classic friction pendulum bearing with same parameters. Equivalent friction force of SLDFPB increases and equivalent inertia force decreases.

2 SLDFPB can maintain its mechanical property even if several columns separate from spherical shell caused by enormous deformation of isolation layer or bad contact of sliding block. Local failure only leads to redistribution of bearing reaction. SLDFPB has stable performance of mechanical property.

3 SLDFPB has sufficient horizontal deformation capability, large vertical carrying capacity, small horizontal stiffness and great isolation effectiveness. Small friction coefficient of spherical surface and small depth of SLDFPB is optimal design strategy considering seismic resistance of structures, safety of isolation layer and resilient ability.

4 Two resilient-isolated structural systems combined isolation with energy-dissipation technique are studied. Large ratio of mass and optimised parameters contributes to good isolation effect. Seismic performance of isolation system is significantly affected by design strategy of isolation layers.

Acknowledgements

This research is supported by the National Key Research and Development Program of China with Grant No. 2017YFC0703603.

References

Almazán, J.L., de la Llera, J.C. and Inaudi, J.A. (1998) 'Modelling aspects of structures isolated with the frictional pendulum system', *Earthquake Engineering & Structural Dynamics*, Vol. 27, No. 8, pp.845–867.

Becker, T.C. and Mahin, S.A. (2012) 'Experimental and analytical study of the bi-directional behavior of the triple friction pendulum isolator', *Earthquake Engineering & Structural Dynamics*, Vol. 41, No. 3, pp.355–373.

Calvi, P.M., Moratti, M. and Calvi, G.M. (2016) 'Seismic isolation devices based on sliding between surfaces with variable friction coefficient', *Earthquake Spectra*, Vol. 32, No. 4, pp.2291–2315.

Chopra, A.K. (2001) *Dynamics of Structures*, 2nd ed., Prentice-Hall, Saddle River NJ,USA.

Dao, N.D., Ryan, K.L., Sato, E. and Sasaki, T. (2013) 'Predicting the displacement of triple pendulum™ bearings in a full-scale shaking experiment using a three-dimensional element', *Earthquake Engineering & Structural Dynamics*, Vol. 42, No. 11, pp.1677–1695.

Du, Y. and Li, H. (2011) 'Numerical analysis on overturning resistant property of seismic isolated building subject to bi-directional earthquake excitation', *Computer Aided Engineering*, Vol. 20, No. 1, pp.1–42.

Fenz, D.M. and Constantinou, M.C. (2006) 'Behaviour of the double concave friction pendulum bearing', *Earthquake Engineering & Structural Dynamics*, Vol. 35, No. 11, pp.1403–1424.

Fenz, D.M. and Constantinou, M.C. (2008a) 'Spherical sliding isolation bearings with adaptive behavior: Experimental verification', *Earthquake Engineering & Structural Dynamics*, Vol. 37, No. 2, pp.185–205.

Fenz, D.M. and Constantinou, M.C. (2008b) 'Bing triple friction pendulum bearings for response-history analysis', *Earthquake Spectra*, Vol. 24, No. 4, pp.1011–1028.

Ghobarah, A. and Ali, H.M. (1988) 'Seismic performance of highway bridges', *Engineering Structures*, Vol. 10, No. 3, pp.157–166.

Landi, L., Grazi, G. and Diotallevi, P.P. (2016) 'Comparison of different models for friction pendulum isolators in structures subjected to horizontal and vertical ground motions', *Soil Dynamics and Earthquake Engineering*, Vol. 81, No. 1, pp.75–83.

Loghman, V., Khoshnoudian, F. and Banazadeh, M. (2015) 'Effect of vertical component of earthquake on seismic responses of triple concave friction pendulum base-isolated structures', *Journal of Vibration and Control*, Vol. 21, No. 11, pp.2099–2113.

Morgan, T.A. and Mahin, S.A. (2010) 'Achieving reliable seismic performance enhancement using multi-stage friction pendulum isolators', *Earthquake Engineering & Structural Dynamics*, Vol. 39, No. 13, pp.1443–1461.

Mosqueda, G., Whittaker, A.S. and Fenves, G.L. (2004) 'Characterization and modeling of friction pendulum bearings subjected to multiple components of excitation', *Journal of Structural Engineering*, Vol. 130, No. 3, pp.433–442.

Murnal, P. and Sinha, R. (2002) 'Earthquake resistant design of structures using the variable frequency pendulum isolator', *Journal of Structural Engineering*, Vol. 128, No. 7, pp.870–880.

Murnal, P. and Sinha, R. (2004) 'Behavior of torsionally coupled structures with variable frequency pendulum isolator', *Journal of Structural Engineering*, Vol. 130, No. 7, pp.1041–1054.

Panchal, V.R. and Jangid, R.S. (2009) 'Seismic response of structures with variable friction pendulum system', *Journal of Earthquake Engineering*, Vol. 13, No. 2, pp.193–216.

Pranesh, M. and Sinha, R. (2000) 'VFPI: an isolation device for aseismic design', *Earthquake Engineering & Structural Dynamics*, Vol. 29, No. 5, pp.603–627.

Standard Institute of Chinese Construction (2001) *Technical Specification for Seismic-Isolation with Laminated Rubber Bearing Isolators*, Technical specification enacted by the Standard Institute of Chinese Construction, China.

Tsai, C.S., Chiang, T.C. and Chen, B.J. (2003) 'Finite element formulations and theoretical study for variable curvature friction pendulum system', *Engineering Structures*, Vol. 25, No. 14, pp.1719–1730.

Tsai, C.S., Chiang, T.C. and Chen, B.J. (2005) 'Experimental evaluation of piecewise exact solution for predicting seismic responses of spherical sliding type isolated structures', *Earthquake Engineering & Structural Dynamics*, Vol. 34, No. 9, pp.1027–1046.

Tsai, C.S., Lin, Y.C. and Su, H.C. (2010) 'Characterization and modeling of multiple friction pendulum isolation system with numerous sliding interfaces', *Earthquake Engineering & Structural Dynamics*, Vol. 39, No. 13, pp.1463–1491.

Wu, P. and Ou, J. (2015) 'Seismic performance analysis and design of high-rise structures under super-strong earthquake', *6th International Conference on Advances in Experimental Structural Engineering*, UIUC, USA.

Zayas, V.A., Low, S.A., Bozzo, L. and Mahin, S.A. (1989) *Feasibility and Performance Studies on Improving the Earthquake Resistance of New and Existing Buildings Using the Friction Pendulum System*, Earthquake Engineering Research Center, Berkeley, CA,USA.

Zayas, V.A., Low, S.S. and Mahin, S.A. (1990) 'A simple pendulum technique for achieving seismic isolation', *Earthquake Spectra*, Vol. 6, No. 2, pp.317–333.